sustainability

MDPI

Article

Green Synthesis of Nickel and Copper Nanoparticles Doped with Silver from *Hammada scoparia* Leaf Extract and Evaluation of Their Potential to Inhibit Microorganisms and to Remove Dyes from Aqueous Solutions

Omayma Bouzekri [1], Sabah El Gamouz [1], Abdelaziz Ed-Dra [2,*], Hamou Moussout [3], Younes Dehmani [4], Hamid Ziyat [4], Mostafa El Idrissi [1], M'barek Choukrad [1] and Sadik Abouarnadasse [4]

[1] Laboratory of Molecular Chemistry and Natural Substances, Faculty of Sciences, Moulay Ismail University of Meknes, Meknes 50000, Morocco
[2] Laboratory of Engineering and Applied Technologies, Higher School of Technology, M'ghila University Campus, Sultan Moulay Slimane University, BP: 591, Beni Mellal 23000, Morocco
[3] Laboratory of Advanced Materials and Process Engineering, Faculty of Sciences, University Ibn Tofail, PB: 133, Kenitra 14000, Morocco
[4] Laboratory of Chemistry-Biology Applied to the Environment, Faculty of Sciences, Moulay Ismail University of Meknes, Meknes 50070, Morocco
* Correspondence: abdelaziz_iaa@yahoo.fr

Abstract: *Hammada scoparia* (Pomel) is a powerful plant with important biological properties. In this study, we report on the green synthesis of silver-doped nickel and copper nanoparticles (NPs) in the presence of *H. scoparia* leaf extract using a self-propagating sol–gel autocombustion process. The synthesized NiO, CuO, Ag-NiO, and Ag-CuO NPs were characterized with Fourier transform infrared spectroscopy (FTIR) and X-ray diffraction (XRD). Afterward, they were tested for their antimicrobial activity as well as their potential to remove dyes from aqueous solutions using adsorption processes for malachite green (MG) and photocatalytic degradation for methylene blue (MB). Our results showed that the mass of the adsorbent had a significant effect on the adsorption rate, which increased to reach a maximum value of 98%. The Ag-CuO NP showed the best final conversion of MB (97.95%) compared to NiO, CuO, and Ag-NiO. In addition, we noted that the NPs doped with silver had the best performance in the removal of dyes. These results indicated that the photocatalytic performance was significantly improved after the addition of silver. Moreover, the antimicrobial activity showed that the studied NPs had moderate activity against the tested bacteria and a weak activity or were ineffective against *Candida albicans*. Therefore, the green synthesis of NPs from *H. scoparia* leaf extract is considered a sustainable alternative to removing dyes from aqueous solutions. However, further investigation should be performed on the other dyes to understand the overall effectiveness of these NPs.

Keywords: *Hammada scoparia*; nanoparticles; methylene blue; malachite green; adsorption; photodegradation; antimicrobial activity

Citation: Bouzekri, O.; El Gamouz, S.; Ed-Dra, A.; Moussout, H.; Dehmani, Y.; Ziyat, H.; El Idrissi, M.; Choukrad, M.; Abouarnadasse, S. Green Synthesis of Nickel and Copper Nanoparticles Doped with Silver from *Hammada scoparia* Leaf Extract and Evaluation of Their Potential to Inhibit Microorganisms and to Remove Dyes from Aqueous Solutions. *Sustainability* **2023**, *15*, 1541. https://doi.org/10.3390/su15021541

Academic Editors: Jarosław Chwastowski and Paweł Staroń

Received: 14 December 2022
Revised: 9 January 2023
Accepted: 11 January 2023
Published: 13 January 2023

1. Introduction

Green synthesis has become a major topic of interest in the field of nanotechnology [1]. Developments in nanotechnology have led to the production of innovative materials [2], particularly ecofriendly nanostructure synthetic procedures used to synthesize metal and metal oxide nanomaterials of any shape and size [3]. Nanomaterials are known for their optical, physicochemical, and biological properties [4,5]. Recent studies have proved the effectiveness of using nanomaterials in different aspects of life, including environmental control, energy storage, solar cells, biomarking, bioprobes, tissue engineering, cancer therapy, cancer diagnosis, and drug delivery [6].

Biosynthetic methods using plant extracts to synthesize nanoparticles (NPs) are currently used on a large scale worldwide [7]. The utilization of plant extracts in NP synthesis is due to the presence of bioactive compounds, which greatly contribute to the potential of reducing NPs' abilities, and give additional properties to the final hybrid materials [8]. This synthesis procedure increases the biocompatibility of the resulting NPs. Consequently, these new bioconjugates could then be used in different fields [9]. In the biological field, the coordination of NPs with biological entities (e.g., microorganisms) has created a succession of nanoparticle–biology interfaces that depend on both colloidal forces and dynamic biophysical and biochemical interactions [10]. In the environmental field, the green synthesis of NPs has been used to control environmental pollution, such as with the degradation of organic dyes and chlorinated organic pollutants, heavy metal removal, in addition to the treatment of wastewater [11].

The species *Haloxylon scoparium* Pomel (Syn. *Hammada scoparia* (Pomel) Iljin) belongs to the most important genus (*Haloxylon*) of the family Amaranthaceae [12], and grows wild in the desert and semidesert areas in the Mediterranean and the Near East regions [13]. In Morocco, it is locally known as Rremt or remeth [14]. This species has several uses in the phytotherapy field [15]. *H. scoparium* has been reported in previous pharmacological studies to have anticancer properties [16], hepatoprotective effects, molluscicidal, cytotoxic, antimalarial, and larvicidal activity [17], in addition to antimicrobial, and antioxidant activity [18]. These biological and pharmacological properties are due to the presence of many heterocyclic compounds in the chemical composition of *H. scoparium* extracts, such as alkaloids carnegine, N-methylisosalsoline, N-omega-methyltryptamine, tryptamine, N-omega-methyltryptamine, beta carboline, isoquinolines, isosalsoline, salsolidine, dehydrosalsolidine, and isosalsolidine [19], and flavonoids, such as isorhamnetin-3-O-beta-D-robinobioside, galactose, and quercetin–glucose–rhamnose [14]. To the best of our knowledge, there are no studies on the syntheses of NPs from *H. scoparium* extracts.

During the last several decades, the resistance of microorganisms to antibiotics has been considered a major threat to public health worldwide. In fact, the World Health Organization has triggered the alarm signal for the research of new substances that are able to treat antimicrobial-resistant microorganisms. In this regard, several research works have been developed to evaluate the antimicrobial activity of new substances and compounds [20,21]. Indeed, research works based on the green synthesis of NPs could be a sustainable alternative to fight against multidrug-resistant bacteria [22–24].

Recently, water pollution has begun to take on more worrying dimensions. Considering this problem, new and cost-effective research based on cutting-edge and ecofriendly techniques is being used to develop new and effective materials for the depollution of aqueous solutions, especially those obtained from textile industries, which are difficult to treat using biological processes. In this regard, adsorption and photocatalysis are considered the best and the most effective techniques for treating aqueous solutions contaminated with organic pollutants [25,26].

Hence, in this work, we aim to study the adsorption capacity and catalytic potential of the green synthesis of nickel and copper NPs doped with silver from *H. scoparium* extract in order to remove methylene blue and malachite green from aqueous solutions. Moreover, we present the first example of using these NPs to combat different microorganisms.

2. Materials and Methods

2.1. Green Synthesis of NiO/CuO and Ag-Doped NiO/CuO NPs

The leaves of *H. scoparium* Pomel (Amaranthaceae) were harvested in May 2019 from the Errachidia region, located in the southeast of Morocco. The vegetal material was dried for 15 days in the dark to avoid the photodegradation of phytochemical compounds by light and, then, was powdered by using an electronic mixer. The green synthesis of NPs was conducted following the protocol described previously by Babu and Antony [5].

2.2. Characterizations

The characterization of NPs was conducted using a Fourier transform infrared (FTIR) spectrometer (Shimadzu, JASCO 4100) with a record range varying between 400 and 4000 cm^{-1} using the KBr pellet technique; in addition, X-ray diffraction (XRD) was conducted using an X'PERT MPD-PRO wide-angle X-ray powder diffractometer fitted with a diffracted beam monochromator and Ni-filtered CuK (source (λ = 1.5418 Å).

2.3. Photocatalytic Degradation

The photocatalytic degradation of dyes using the synthesized NPs (NiO, CuO, Ag-NiO, and Ag-CuO) wad performed in a homemade photoreactor following the protocol described previously [5], with a few modifications. Briefly, the aqueous solution of MB (100 mL; 10 mg/L) containing 100 mg of the photocatalyst was kept in the dark to reach equilibrium and stirred for 30 min, followed by the addition of 0.1 mL of H_2O_2. The mixture was subjected to white light irradiation in the photoreactor. The evaluation of the photodegradation efficiency was ensured by sampling 3 mL of solution at regular time intervals (5 min) and measuring spectrophotometrically for their absorbances. Finally, the efficiency of photodegradation was calculated based on Equation (1) [27]:

$$R(\%) = \frac{C_0 - C_t}{C_0} \times 100 \quad (1)$$

where C_0 and C_t are the initial and the final (after t time in minutes) concentrations of dye in mg/L.

2.4. Adsorption Studies of Ag/CuO

The adsorption of MG on the synthesized NPs was evaluated under different factors, including temperature, adsorbent dose, contact time, pH, and initial dye concentration. The experiments were performed by shaking the catalysts with 200 mL of MG (10 mg/L) in an orbital shaker at 150 rpm until reaching equilibrium. Then, the absorbance of the supernatant of the MG solution was measured at 617 nm, and the amount of the adsorbed MG (mg dye/g adsorbent) and the adsorption percentage were calculated following Equations (2) and (3):

$$R(\%) = \frac{C_0 - C_e}{C_0} \times 100 \quad (2)$$

$$Q = \frac{C_0 - C_e}{m} \times V \quad (3)$$

where C_0 is the initial MG concentration (mg/L); C_e is the concentration of the unabsorbed MG (mg/L); m is the amount of catalyst (g); V is the volume of the MG solution (L); Q is the amount of MG adsorbed per gram of catalyst (mg/g).

2.5. Antimicrobial Assay

The antimicrobial activity of the studied NPs was evaluated against 4 bacterial strains (*Escherichia coli* ATCC 25922, *Staphylococcus* aureus, *Salmonella* Typhimurium, and *Enterococcus faecalis)* belonging to Gram-positive and Gram-negative bacteria, and one yeast strain (*Candida albicans*). *S.* Typhimurium and *S. aureus* were isolated from meat products [28,29], while *E. faecalis* and *C. albicans* were obtained from the Regional Hospital of Meknes (Mohammed V Hospital, Morocco). Before use, bacterial strains were revivified with subcultures in tryptone soya agar (TSA, Biokar, Beauvais, France) at 37 °C for 24 h, while yeast was revivified with subcultures in Sabouraud dextrose agar with chloramphenicol (Biokar, Beauvais, France) at 25 °C for 48 h. Then, a microbial suspension equivalent to 0.5 McFarland (108 cfu/mL) was prepared in sterile physiological water (0.9% NaCl) and inoculated by swabbing on plates containing Mueller–Hinton agar (Biokar, Beauvais, France) [30]. On the surface of each plate, 10 µL of each NP solution at a concentration of 10 µg/mL was dropped on 6 mm diameter filter paper discs (Whatman Grade 4 Qualitative

Filter Papers, Merck, Germany. Sterile distilled water (10 µL) was used as a negative control, while gentamicin (30 µg) was used as a positive control for bacteria and 10 µL of Canaflucan (fluconazole) Win® capsule 150 mg with a concentration of 0.6 µg/mL was used as a positive control for the yeast strain. The used plates were incubated at 37 °C for 18–24 h for bacteria and 25 °C for 44–48 °C for yeast. After incubation, the inhibition diameter was measured in millimeters (disk included) [30]. The antimicrobial activity was classified into three levels based on the produced inhibitory diameter: weak (inhibition zone $\leq$ 12.0 mm), intermediate/moderate (12.1 mm $\leq$ inhibition zone $\leq$ 20.0 mm), and strong (inhibition zone $\geq$ 20.1 mm).

2.6. Statistical Analysis

Origin software and Microsoft Excel were used for the generation of figures and the statistical analysis. In this study, the experiments were carried out in triplicate, and the difference between groups was determined by using the Student *t*-test ($p < 0.05$).

3. Results and Discussion

3.1. Characterization of NPs

3.1.1. FTIR

FTIR spectra show band characteristics of the metal oxygenate and bands assigned to the hydroxyl group, which originated from water, and bands from the C-O carbon dioxide bond, which originated from the air (Figure 1). Indeed, the 3430 and 1380 cm^{-1} bands characterized the vibration of the H-O and H-O-H bonds [31]; the 2920 and 1320 cm^{-1} bands are characteristic bands of CO_2 [31]. The characteristic bands of silver appeared in 1658, 1430, and 1136 cm^{-1} [32], and the vibration of the Cu-O bond appeared at 629, 827, 663, and 513 cm^{-1} [32]. Finally, the bands at 496, 423, 440, and 470 cm^{-1} were attributed to the vibration of the Ni-O bond [33]. The appearance of these bonds confirmed that there were interactions between the metals and the plant extract powder when forming the NPs.

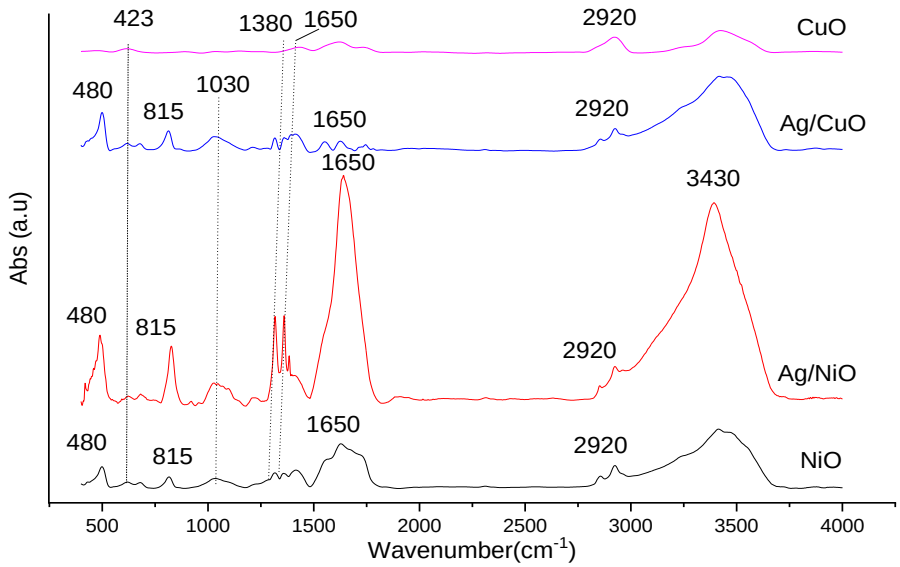

Figure 1. FTIR spectra of CuO, Ag-CuO, Ag-NiO, and NiO.

3.1.2. XRD

The diffraction patterns of the synthesized copper and nickel NPs obtained from the metal nitrates and the plant extracts showed sharp and intense peaks, which clearly indicated that the particles were crystalline. The representative X-ray diffraction pattern is shown in Figure 2. All of the reflections could be indexed in face-centered cubic (FCC) with a constant in the network (a): 4.175 A (space group Fm 3 hm (2 2 5)) [31,34], which was consistent with standard data (JCPDS card no. 47-1049). The XRD spectrum of CuO, NiO,

Ag-CuO, and Ag-NiO NPs is shown in Figure 2. The NPs gave diffraction peaks of 2θ and Miller indices of 34.7, 36.9, 39.3, 48.0, 56.3, and 66.8, which were attributed to (1 1 0), (11–1), (1 1 1), (20–2), (2 0 2), and (0 2 2), respectively. The peaks corresponded to a monoclinic structure, which agreed very well with the standard lattice parameters of a = 4.6490 Å, b = 3.4382 Å, and c = 5.1870 Å, as determined by the JCPDS card no. 96–901-5925, shown in Figure 2 [35].

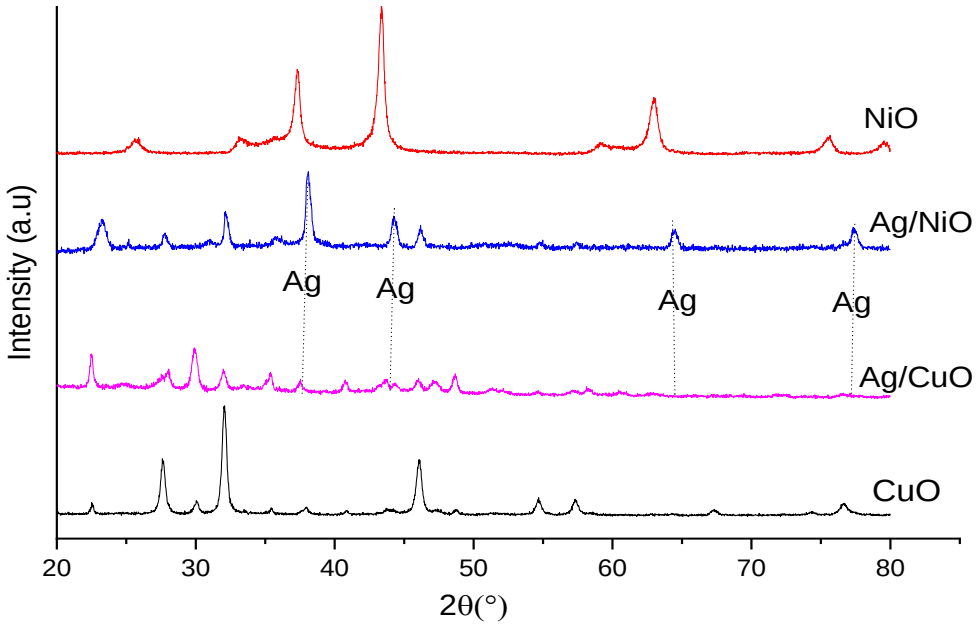

Figure 2. XRD spectra of CuO, Ag-CuO, Ag-NiO, and NiO.

3.2. Adsorption Study

3.2.1. Effect of pH and Mass of Adsorbent

The pH and mass of the adsorbent are essential parameters in the adsorption process. Indeed, the pH influences the surface charge, the degree of ionization, and the dissociation of functional groups at the active sites of the adsorbent. Particularly, the pH is known to affect the structural stability of MG and, therefore, its color intensity [36]. The molecule of MG was protonated in the acidic medium and deprotonated at a higher pH; as a result, it had a high density of positive charges at a lower pH. Figure 3 shows that when the pH increased, the yield underwent a significant increase, which suggests that the adsorption of MG is favorable in a basic medium; this characteristic shows that the molecules of MG are linked with the negative sites of solids (m), thanks to the effect of the pH on the dominant charge on the surface. These results were in agreement with previous findings [37].

Figure 3 shows the effect of the adsorbent mass on the adsorption rate. According to this figure, there was a significant increase that reached a maximum value of 98%; this effect can be justified by the increases in the number of available adsorption sites increasing dose of adsorbent (Ag-CuO), consequently, leading to an increase in the percentage of adsorption of MG.

From Figure 4, the adsorbed amount of dyes (MG and MB) varied as a function of solid NiO and Ag-NiO. This increase depended on the solid doping with silver, which caused a variation in the texture and structure of the solid NiO. The doping of nickel oxide with silver gave different results in the removal of the two organic pollutants, MG and MB, in comparison with the copper oxide doped with silver. These results were in agreement with the results quoted in the literature [38–40].

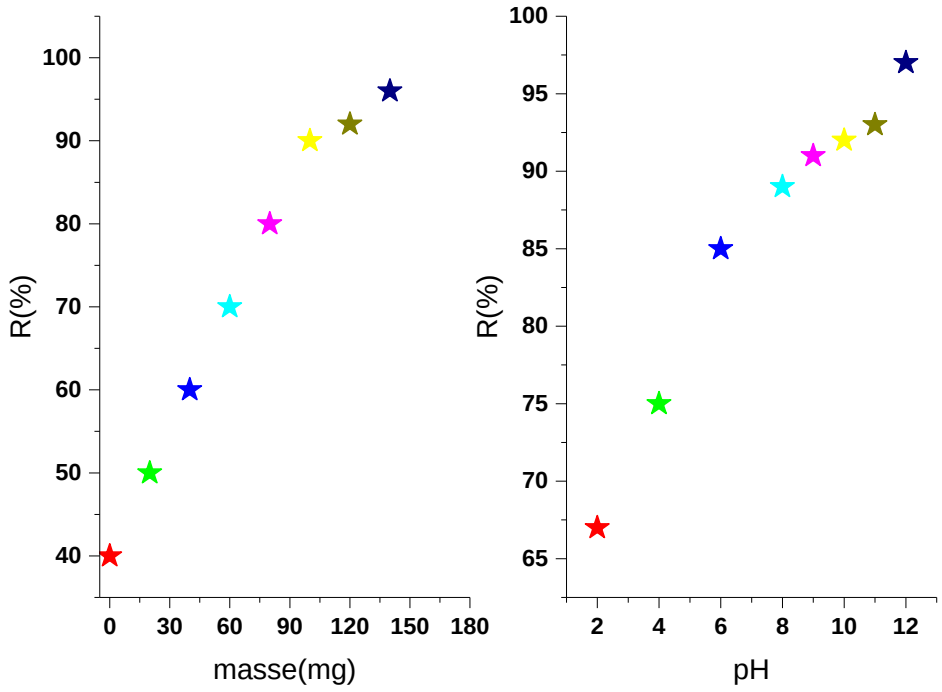

Figure 3. Effect of adsorbent mass and pH on the adsorption of MG onto Ag-CuO.

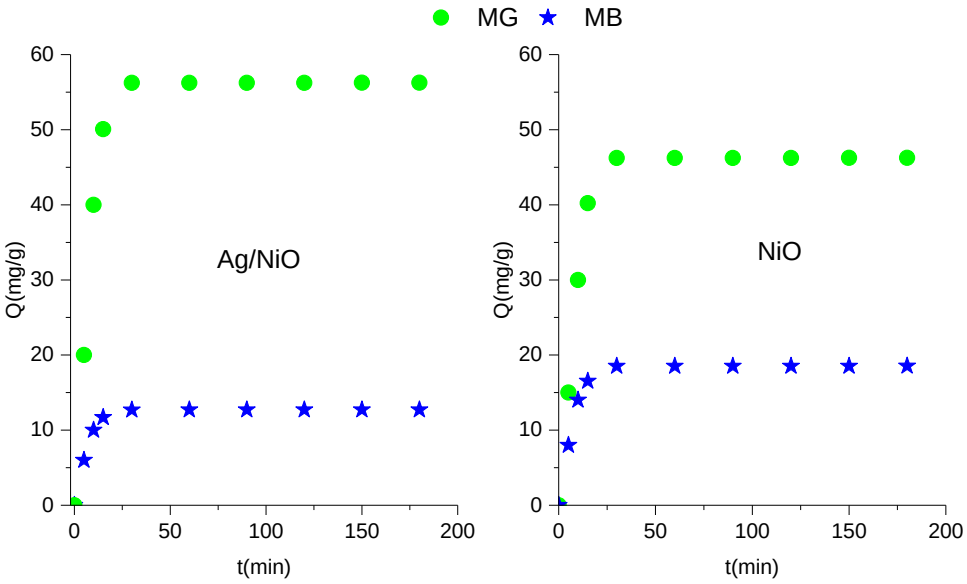

Figure 4. Effect of solid nature on dye adsorption of MG and MB onto NiO and Ag-NiO.

3.2.2. Adsorption Kinetics

From Figure 5, it can be seen that the first-order Lagergren equation was not applicable in the case of the adsorption of MG on Ag-NiO for all three dye concentrations. On the other hand, according to Figure 5, the obtained results perfectly followed the nonlinear variation given by the representative equation of pseudo-second-order kinetics. From the linear regression data of the different models, and based on the values obtained for the correlation coefficients, which were close to unity, and the values of the calculated adsorption capacities, which were close to the experimental ones, it can be concluded that the adsorption kinetics of the dye were better described by the pseudo-second-order model than the first-order one [41,42].

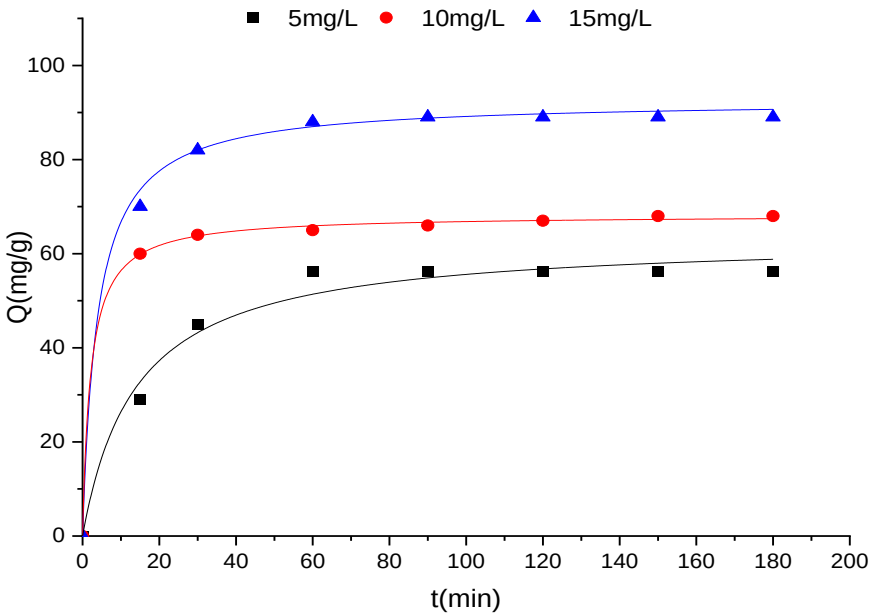

Figure 5. Kinetic adsorption of MG onto Ag-NiO.

According to Figure 6, the adsorbed quantity increased as a function of the temperature; this showed the endothermic character of the adsorption of the dye on the solid. The relation between the temperature and the adsorbed quantity could be justified by the effect of heat on the space between the solid particles. The more the temperature increased, the more the heat increased automatically in terms of energy, which then increased the possibility of an interaction occurring between the molecules of the adsorbate and the particles of the increased adsorbent [43,44].

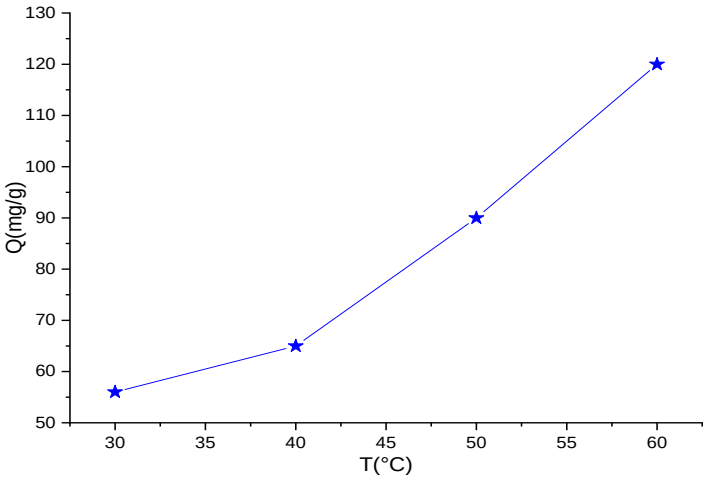

Figure 6. Temperature effect on adsorption of MG onto Ag-NiO.

3.3. Photodegradation

The photocatalytic activity of the synthesized NPs was probed in the presence of visible light using the blue solution as a molecular probe. The results obtained were expressed as a percentage of MB removed, as shown in Figure 7. To ensure that the reaction proceeded only in the presence of light and a photocatalyst, the MB solution was tested under visible light for 3 h in the absence of a photocatalyst. The results showed no concentration changes (negligible changes), suggesting that the obtained results were due to the simultaneous presence of a photocatalyst and light.

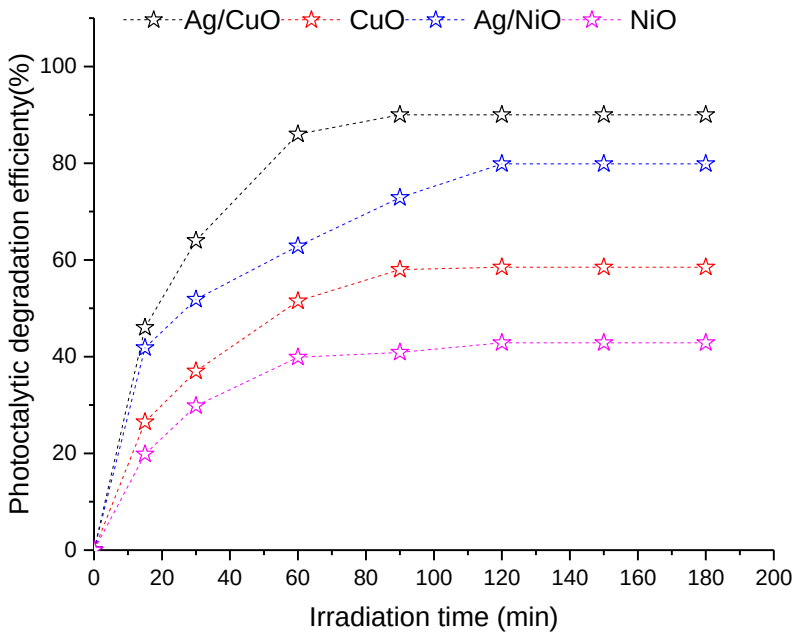

Figure 7. Photocatalytic degradation efficiency of MB in the presence of NiO, CuO, Ag-NiO, and Ag-CuO. Dose of NPs (m = 0.2 g), C_0 (MB) = 10^{-5} mol/L.

Figure 7 shows the elimination curves of MB as a function of the irradiation time under visible light in the presence of the studied materials (NiO and CuO) and the solids doped with silver (Ag-NiO and Ag-CuO). It is clear from the photolysis curves (experiments in the dark) that under visible light, the presence of a photocatalyst was necessary to initiate the photocatalytic reaction [45]. As shown in Figure 7, under UV light, the Ag-CuO sample showed the best final conversion of MB (97.95%) compared to NiO, CuO, and Ag-NiO. In addition, we noted that the NPs doped with silver had the best performance in the removal of dyes. These results indicated that the photocatalytic performance was significantly improved after the addition of silver. These results showed a large effect of doping on the structural and textural properties of the NPs, an effect shown in the comparison between the removal efficiency between CuO and Ag-CuO. This effect can be justified with the creation of new active sites on the catalyst surface. These results were confirmed by other works in the literature [46,47].

3.4. Antimicrobial Activity

The antimicrobial activity of the studied NPs was performed against four bacterial strains (*E. coli*, *S*. Typhimurium, *S. aureus*, and *E. faecalis*) and one yeast strain (*C. albicans*), using the disc diffusion method, with the results presented in Figure 8. The results of this study showed that the studied NPs had moderate to weak activity against the tested bacteria and weak activity against *C. albicans*. The NPs CuO and Ag-CuO were more effective against Gram-positive bacteria than Gram-negative bacteria, while NiO and Ag-NiO did not depend on the bacterial type. Thus far, several studies have demonstrated the antimicrobial activity of the "green" synthesis of silver, copper, and nickel NPs [48–50], while, to our knowledge, this was the first study that described the antimicrobial activity of NPs synthesized from *H. scoparium*. More importantly, the antimicrobial mechanisms of NPs are not completely understood, but it was supposed that there are different ways to combat microorganisms [20]. In fact, the combined effect of different NPs with other antimicrobial substances, such as antibiotics, essential oils, etc., could improve the antimicrobial effectiveness of NPs [20,51,52].

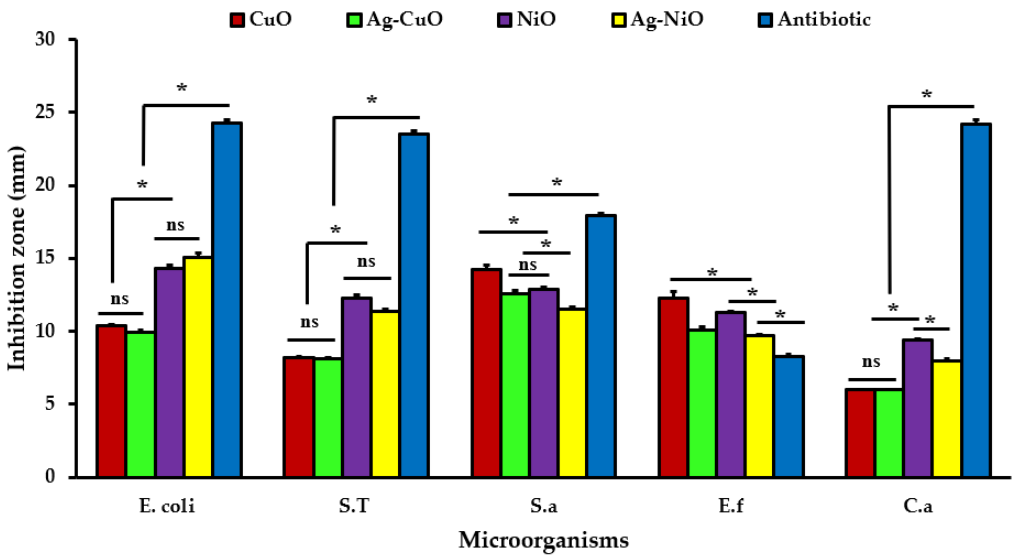

Figure 8. Inhibition zones of the studied NPs against the tested bacteria. *E. coli*: *Escherichia coli* ATCC 25922; S.T: *Salmonella* Typhimurium; S.a: *Staphylococcus aureus*; E.f: *Enterococcus faecalis*; C.a: *Candida albicans*; ns: no significant difference; *: significant different ($p < 0.05$).

4. Conclusions

In this study, transition metal oxide NPs were successfully prepared using a simple and environmentally friendly procedure. Furthermore, we reported that the use of natural and economical reducing agents, such as the plant *H. scoparia,* could produce metal nanostructures in an aqueous solution, avoiding the presence of toxic reagents. The NPs synthesized in this work showed a significant increase in the effect of adsorbent mass on the adsorption rate, reaching a maximum value of 98%. Moreover, we found that the photocatalytic performance was significantly improved after the addition of silver. The results of the antimicrobial activity of the studied NPs showed moderate activity against the tested bacteria and weak activity against the studied yeast. Therefore, green synthesis processes could be used as an ecofriendly method to synthesize NPs of high interest for the removal of dyes from aqueous solutions and combatting multidrug-resistant bacteria. However, in respect of this study, we plan to evaluate the performance of other combinations of NPs in enhancing their ability to remove dyes and combat multidrug-resistant microorganisms.

Author Contributions: Conceptualization, M.E.I., M.C. and S.A.; methodology, A.E-D., H.M. and Y.D.; software, H.M., Y.D. and H.Z.; validation, A.E-D., M.E.I., M.C. and S.A.; formal analysis, O.B., S.E.G., H.M., Y.D. and H.Z.; investigation, O.B., S.E.G. and A.E.-D.; resources, M.E.I., M.C. and S.A.; data curation, O.B., S.E.G. and Y.D.; writing—original draft preparation, O.B. and S.E.G.; writing—review and editing, A.E.-D., H.M. and Y.D.; supervision, M.E.I., M.C. and S.A. All authors have read and agreed to the published version of the manuscript.

Funding: This research received no external funding.

Institutional Review Board Statement: Not applicable.

Informed Consent Statement: Not applicable.

Data Availability Statement: Not applicable.

Acknowledgments: The authors are grateful to the anonymous reviewers for their valuable comments and suggestions.

Conflicts of Interest: The authors declare no conflict of interest.

References

1. Shebl, A.; Hassan, A.A.; Salama, D.M.; Abd El-Aziz, M.E.; Abd Elwahed, M.S.A. Green Synthesis of Nanofertilizers and Their Application as a Foliar for Cucurbita Pepo l. *J. Nanomater.* **2019**, *2019*, 3476437. [CrossRef]
2. Fuku, X.; Modibedi, M.; Mathe, M. Green Synthesis of Cu/Cu2O/CuO Nanostructures and the Analysis of Their Electrochemical Properties. *SN Appl. Sci.* **2020**, *2*, 902. [CrossRef]
3. Shankar, S.S.; Ahmad, A.; Sastry, M. Geranium Leaf Assisted Biosynthesis of Silver Nanoparticles. *Biotechnol. Prog.* **2003**, *19*, 1627–1631. [CrossRef] [PubMed]
4. Singh, R.P. Prospects of Nanobiomaterials for Biosensing. *Int. J. Electrochem.* **2011**, *2011*, 125487. [CrossRef]
5. Babu, A.T.; Antony, R. Green Synthesis of Silver Doped Nano Metal Oxides of Zinc & Copper for Antibacterial Properties, Adsorption, Catalytic Hydrogenation & Photodegradation of Aromatics. *J. Environ. Chem. Eng.* **2019**, *7*, 102840. [CrossRef]
6. Mandal, G.; Ganguly, T. Applications of Nanomaterials in the Different Fields of Photosciences. *Indian J. Phys.* **2011**, *85*, 1229–1245. [CrossRef]
7. Chandran, S.P.; Chaudhary, M.; Pasricha, R.; Ahmad, A.; Sastry, M. Synthesis of Gold Nanotriangles and Silver Nanoparticles Using Aloevera Plant Extract. *Biotechnol. Prog.* **2006**, *22*, 577–583. [CrossRef]
8. Jadhav, K.; Dhamecha, D.; Bhattacharya, D.; Patil, M. Green and Ecofriendly Synthesis of Silver Nanoparticles: Characterization, Biocompatibility Studies and Gel Formulation for Treatment of Infections in Burns. *J. Photochem. Photobiol. B* **2016**, *155*, 109–115. [CrossRef]
9. Khan, I.; Saeed, K.; Khan, I. Nanoparticles: Properties, Applications and Toxicities. *Arab. J. Chem.* **2019**, *12*, 908–931. [CrossRef]
10. Ranoszek-Soliwoda, K.; Tomaszewska, E.; Małek, K.; Celichowski, G.; Orlowski, P.; Krzyzowska, M.; Grobelny, J. The Synthesis of Monodisperse Silver Nanoparticles with Plant Extracts. *Colloids Surf. B Biointerfaces* **2019**, *177*, 19–24. [CrossRef]
11. Saif, S.; Tahir, A.; Chen, Y. Green Synthesis of Iron Nanoparticles and Their Environmental Applications and Implications. *Nanomaterials* **2016**, *6*, 209. [CrossRef] [PubMed]
12. Taïr, K.; Kharoubi, O.; Taïr, O.A.; Hellal, N.; Benyettou, I.; Aoues, A. Aluminium-Induced Acute Neurotoxicity in Rats: Treatment with Aqueous Extract of Arthrophytum (*Hammada scoparia*). *J. Acute Dis.* **2016**, *5*, 470–482. [CrossRef]
13. Boulanouar, B.; Abdelaziz, G.; Aazza, S.; Gago, C.; Miguel, M.G. Antioxidant Activities of Eight Algerian Plant Extracts and Two Essential Oils. *Ind. Crops Prod.* **2013**, *46*, 85–96. [CrossRef]
14. Kharchoufa, L.; Bouhrim, M.; Bencheikh, N.; el Assri, S.; Amirou, A.; Yamani, A.; Choukri, M.; Mekhfi, H.; Elachouri, M. Acute and Subacute Toxicity Studies of the Aqueous Extract from Haloxylon Scoparium Pomel (*Hammada scoparia* (Pomel)) by Oral Administration in Rodents. *Biomed. Res. Int.* **2020**, *2020*, 4020647. [CrossRef]
15. Haida, S.; Kribii, A. Chemical Composition, Phenolic Content and Antioxidant Capacity of Haloxylon Scoparium Extracts. *S. Afr. J. Bot.* **2020**, *131*, 151–160. [CrossRef]
16. Bourogaa, E.; Bertrand, J.; Despeaux, M.; Jarraya, R.; Fabre, N.; Payrastre, L.; Demur, C.; Fournié, J.J.; Damak, M.; Feki, A.; et al. Hammada Scoparia Flavonoids and Rutin Kill Adherent and Chemoresistant Leukemic Cells. *Leuk. Res.* **2011**, *35*, 1093–1101. [CrossRef]
17. Bouaziz, A.; Mhalla, D.; Zouari, I.; Jlaiel, L.; Tounsi, S.; Jarraya, R.; Trigui, M. Antibacterial and Antioxidant Activities of Hammada Scoparia Extracts and Its Major Purified Alkaloids. *S. Afr. J. Bot.* **2016**, *105*, 89–96. [CrossRef]
18. Lamchouri, F.; Benali, T.; Bennani, B.; Toufik, H.; Ibn, L.; Hassani, M.; Bouachrine, M.; Lyoussi, B.; Ben, M.; Maroc, A. Preliminary Phytochemical and Antimicrobial Investigations of Extracts of Haloxylon Scoparium. *J. Mater. Environ. Sci* **2012**, *3*, 754–759.
19. El-Shazly, A.; Wink, M. Tetrahydroisoquinoline and β-Carboline Alkaloids from Haloxylon Articulatum (Cav.) Bunge (Chenopodiaceae). *Z. Fur Nat.—Sect. C J. Biosci.* **2003**, *58*, 477–480. [CrossRef]
20. Wang, L.; Hu, C.; Shao, L. The Antimicrobial Activity of Nanoparticles: Present Situation and Prospects for the Future. *Int. J. Nanomed.* **2017**, *12*, 1227–1249. [CrossRef]
21. Ed-Dra, A.; Nalbone, L.; Filali, F.R.; Trabelsi, N.; el Majdoub, Y.O.; Bouchrif, B.; Giarratana, F.; Giuffrida, A. Comprehensive Evaluation on the Use of Thymus Vulgaris Essential Oil as Natural Additive against Different Serotypes of Salmonella Enterica. *Sustainability* **2021**, *13*, 4594. [CrossRef]
22. Zhu, X.; Pathakoti, K.; Hwang, H.-M. Green Synthesis of Titanium Dioxide and Zinc Oxide Nanoparticles and Their Usage for Antimicrobial Applications and Environmental Remediation. In *Green Synthesis, Characterization and Applications of Nanoparticles*; Elsevier: Amsterdam, The Netherlands, 2019; pp. 223–263.
23. Hussain, I.; Singh, N.B.; Singh, A.; Singh, H.; Singh, S.C. Green Synthesis of Nanoparticles and Its Potential Application. *Biotechnol. Lett.* **2016**, *38*, 545–560. [CrossRef]
24. Castillo-Henríquez, L.; Alfaro-Aguilar, K.; Ugalde-álvarez, J.; Vega-Fernández, L.; de Oca-Vásquez, G.M.; Vega-Baudrit, J.R. Green Synthesis of Gold and Silver Nanoparticles from Plant Extracts and Their Possible Applications as Antimicrobial Agents in the Agricultural Area. *Nanomaterials* **2020**, *10*, 1763. [CrossRef]
25. Gusain, R.; Gupta, K.; Joshi, P.; Khatri, O.P. Adsorptive Removal and Photocatalytic Degradation of Organic Pollutants Using Metal Oxides and Their Composites: A Comprehensive Review. *Adv. Colloid Interface Sci.* **2019**, *272*, 102009. [CrossRef] [PubMed]
26. Reddy, C.V.; Reddy, I.N.; Ravindranadh, K.; Reddy, K.R.; Shetti, N.P.; Kim, D.; Shim, J.; Aminabhavi, T.M. Copper-Doped ZrO2 Nanoparticles as High-Performance Catalysts for Efficient Removal of Toxic Organic Pollutants and Stable Solar Water Oxidation. *J. Environ. Manag.* **2020**, *260*, 110088. [CrossRef] [PubMed]

27. Liu, Z.; Zhang, Y.; Kong, L.; Liu, L.; Luo, J.; Liu, B.; Zhou, Q.; He, F.; Xu, D.; Wu, Z. Preparation and Preferential Photocatalytic Degradation of Acephate by Using the Composite Photocatalyst Sr/TiO2-PCFM. *Chem. Eng. J.* **2019**, *374*, 852–862. [CrossRef]
28. Ed-Dra, A.; Filali, F.R.; Khayi, S.; Oulghazi, S.; Bouchrif, B.; el Allaoui, A.; Ouhmidou, B.; Moumni, M. Antimicrobial Resistance, Virulence Genes, and Genetic Diversity of Salmonella Enterica Isolated from Sausages. *Eur. J. Microbiol. Immunol.* **2019**, *9*, 56–61. [CrossRef] [PubMed]
29. Ed-Dra, A.; Filali, F.R.; Bouymajane, A.; Benhallam, F.; el Allaoui, A.; Chaiba, A.; Giarratana, F. Antibiotic Susceptibility Profile of Staphylococcus Aureus Isolated from Sausages in Meknes, Morocco. *Vet. World* **2018**, *11*, 1459–1465. [CrossRef] [PubMed]
30. Ed-Dra, A.; Filali, F.R.; lo Presti, V.; Zekkori, B.; Nalbone, L.; Bouymajane, A.; Trabelsi, N.; Lamberta, F.; Bentayeb, A.; Giuffrida, A.; et al. Chemical Composition, Antioxidant Capacity and Antibacterial Action of Five Moroccan Essential Oils against Listeria Monocytogenes and Different Serotypes of Salmonella Enterica. *Microb. Pathog.* **2020**, *149*, 104510. [CrossRef] [PubMed]
31. Khaleed, A.A.; Bello, A.; Dangbegnon, J.K.; Momodu, D.Y.; Madito, M.J.; Ugbo, F.U.; Akande, A.A.; Dhonge, B.P.; Barzegar, F.; Olaniyan, O.; et al. Effect of Activated Carbon on the Enhancement of CO Sensing Performance of NiO. *J. Alloys Compd.* **2017**, *694*, 155–162. [CrossRef]
32. Thakur, N.; Anu; Kumar, K. Effect of (Ag, Co) Co-Doping on the Structural and Antibacterial Efficiency of CuO Nanoparticles: A Rapid Microwave Assisted Method. *J. Environ. Chem. Eng.* **2020**, *8*, 104011. [CrossRef]
33. Dehmani, Y.; Abouarnadasse, S. Study of the Adsorbent Properties of Nickel Oxide for Phenol Depollution. *Arab. J. Chem.* **2020**, *13*, 5312–5325. [CrossRef]
34. Behnajady, M.A.; Bimeghdar, S. Synthesis of Mesoporous NiO Nanoparticles and Their Application in the Adsorption of Cr(VI). *Chem. Eng. J.* **2014**, *239*, 105–113. [CrossRef]
35. Ramzan, M.; Obodo, R.M.; Mukhtar, S.; Ilyas, S.Z.; Aziz, F.; Thovhogi, N. Green Synthesis of Copper Oxide Nanoparticles Using Cedrus Deodara Aqueous Extract for Antibacterial Activity. *Mater. Today Proc.* **2021**, *36*, 576–581. [CrossRef]
36. Dehbi, A.; Dehmani, Y.; Omari, H.; Lammini, A.; Elazhari, K.; Abouarnadasse, S.; Abdallaoui, A. Comparative Study of Malachite Green and Phenol Adsorption on Synthetic Hematite Iron Oxide Nanoparticles (α-Fe_2O_3). *Surf. Interfaces* **2020**, *21*, 100637. [CrossRef]
37. Dehmani, Y.; Alrashdi, A.A.; Lgaz, H.; Lamhasni, T.; Abouarnadasse, S.; Chung, I.M. Removal of Phenol from Aqueous Solution by Adsorption onto Hematite (α-Fe_2O_3): Mechanism Exploration from Both Experimental and Theoretical Studies. *Arab. J. Chem.* **2020**, *13*, 5474–5486. [CrossRef]
38. Kundu, A.; Mondal, A. Kinetics, Isotherm, and Thermodynamic Studies of Methylene Blue Selective Adsorption and Photocatalysis of Malachite Green from Aqueous Solution Using Layered Na-Intercalated Cu-Doped Titania. *Appl. Clay. Sci.* **2019**, *183*, 105323. [CrossRef]
39. Kant, S.; Pathania, D.; Singh, P.; Dhiman, P.; Kumar, A. Removal of Malachite Green and Methylene Blue by Fe0.01Ni0.01Zn0.98O/Polyacrylamide Nanocomposite Using Coupled Adsorption and Photocatalysis. *Appl. Catal. B* **2014**, *147*, 340–352. [CrossRef]
40. Luo, X.P.; Fu, S.Y.; Du, Y.M.; Guo, J.Z.; Li, B. Adsorption of Methylene Blue and Malachite Green from Aqueous Solution by Sulfonic Acid Group Modified MIL-101. *Microporous Mesoporous Mater.* **2017**, *237*, 268–274. [CrossRef]
41. Nazir, M.A.; Bashir, M.A.; Najam, T.; Javed, M.S.; Suleman, S.; Hussain, S.; Kumar, O.P.; Shah, S.S.A.; Rehman, A. ur Combining Structurally Ordered Intermetallic Nodes: Kinetic and Isothermal Studies for Removal of Malachite Green and Methyl Orange with Mechanistic Aspects. *Microchem. J.* **2021**, *164*, 105973. [CrossRef]
42. Choudhary, M.; Kumar, R.; Neogi, S. Activated Biochar Derived from Opuntia Ficus-Indica for the Efficient Adsorption of Malachite Green Dye, Cu^{+2} and Ni^{+2} from Water. *J. Hazard. Mater.* **2020**, *392*, 122441. [CrossRef] [PubMed]
43. Zou, J.; Rezaee, R.; Xie, Q.; You, L. Characterization of the Combined e Ff Ect of High Temperature and Moisture on Methane Adsorption in Shale Gas Reservoirs. *J. Pet. Sci. Eng.* **2019**, *182*, 106353. [CrossRef]
44. Liu, Y.; Zhu, Y.; Liu, S.; Li, W.; Tang, X. Temperature Effect on Gas Adsorption Capacity in Different Sized Pores of Coal: Experiment and Numerical Modeling. *J. Pet. Sci. Eng.* **2018**, *165*, 821–830. [CrossRef]
45. Zhang, W.; Camarena, D.C. Development of ZnFe2O4 Nanoparticle Functionalized Baker's Yeast Composite for Effective Removal of Methylene Blue via Adsorption and Photodegradation. *J. Water Process Eng.* **2020**, *37*, 101234. [CrossRef]
46. Phuruangrat, A.; Kuntalue, B.; Thongtem, S.; Thongtem, T. Hydrothermal Synthesis of Hexagonal ZnO Nanoplates Used for Photodegradation of Methylene Blue. *Optik* **2021**, *226*, 165949. [CrossRef]
47. de Oliveira Alves, F.H.; Araújo, O.A.; de Oliveira, A.C.; Garg, V.K. Preparation and Characterization of PAni(CA)/Magnetic Iron Oxide Hybrids and Evaluation in Adsorption/Photodegradation of Blue Methylene Dye. *Surf. Interfaces* **2021**, *23*, 100954. [CrossRef]
48. Din, M.I.; Nabi, A.G.; Rani, A.; Aihetasham, A.; Mukhtar, M. Single Step Green Synthesis of Stable Nickel and Nickel Oxide Nanoparticles from Calotropis Gigantea: Catalytic and Antimicrobial Potentials. *Environ. Nanotechnol. Monit. Manag.* **2018**, *9*, 29–36. [CrossRef]
49. Logeswari, P.; Silambarasan, S.; Abraham, J. Synthesis of Silver Nanoparticles Using Plants Extract and Analysis of Their Antimicrobial Property. *J. Saudi Chem. Soc.* **2015**, *19*, 311–317. [CrossRef]
50. Sharma, P.; Pant, S.; Dave, V.; Tak, K.; Sadhu, V.; Reddy, K.R. Green Synthesis and Characterization of Copper Nanoparticles by Tinospora Cardifolia to Produce Nature-Friendly Copper Nano-Coated Fabric and Their Antimicrobial Evaluation. *J. Microbiol. Methods* **2019**, *160*, 107–116. [CrossRef]

51. Geoprincy, G.; Saravanan, P.; Nagendra Gandhi, N.; Renganathan, S. A Novel Approach for Studying the Combined Antimicrobial Effects of Silver Nanoparticles and Antibiotics through Agar over Layer Method and Disk Diffusion Method. *Dig. J. Nanomater. Biostruct.* **2011**, *6*, 1557–1565.
52. Rai, M.; Paralikar, P.; Jogee, P.; Agarkar, G.; Ingle, A.P.; Derita, M.; Zacchino, S. Synergistic Antimicrobial Potential of Essential Oils in Combination with Nanoparticles: Emerging Trends and Future Perspectives. *Int. J. Pharm.* **2017**, *519*, 67–78. [CrossRef] [PubMed]